Radiocarbon and PMF based source apportionment of $PM_{2.5}$ at a regional background site in North China: insight into the contribution of biomass burning

Zheng Zong[1,6], Xiaoping Wang[2], Chongguo Tian[1,*], Yingjun Chen[3,*], Lin Qu[4], Ling Ji[4], Guorui Zhi[5], Jun Li[2], Gan Zhang[2]

[1] Key Laboratory of Coastal Environmental Processes and Ecological Remediation, Yantai Institute of Coastal Zone Research, Chinese Academy of Sciences, Yantai, 264003, China

[2] State Key Laboratory of Organic Geochemistry, Guangzhou Institute of Geochemistry, Chinese Academy of Sciences, Guangzhou, 510640, China

[3] Key Laboratory of Cities' Mitigation and Adaptation to Climate Change in Shanghai (CMA), College of Environmental Science and Engineering, Tongji University, Shanghai, 200092, China

[4] Yantai Oceanic Environmental Monitoring Central Station, SOA, Yantai, 264006, China

[5] Chinese Research Academy of Environmental Sciences, Beijing, 100012, China

[6] University of Chinese Academy of Sciences, Beijing, 100049, China

* Corresponding author:

Chongguo Tian, Yantai Institute of Coastal Zone Research, CAS. Phone: +86-535-2109-160; Fax: +86-535-2109-000; e-mail: cgtian@yic.ac.cn

Yingjun Chen, College of Environmental Science and Engineering, Tongji University. Phone: +86-535-2109-160; Fax: +86-535-2109-000; e-mail: yjchentj@tongji.edu.cn

Abstract

Source apportionment of fine particles ($PM_{2.5}$) at a background site in North China in the winter of 2014 was assessed via statistical analysis, radiocarbon (^{14}C) measurement, and Positive Matrix Factorization (PMF) modeling. Results showed that the concentration of $PM_{2.5}$ was 77.6 ± 59.3 μg m^{-3}, of which SO_4^{2-} concentration was the highest, followed by NO_3^-, organic carbon (OC), elemental carbon (EC) and NH_4^+, respectively. Demonstrated by backward trajectory, more than half of the air mass during the sampling period was from the Beijing-Tianjin-Hebei (BTH) region, followed by Mongolia and the Shandong Peninsula. Cluster analysis of chemical species showed an obvious signal of biomass burning emission in the $PM_{2.5}$ from the Shandong Peninsula, while the $PM_{2.5}$ from the BTH region showed a vehicle emission pattern. This finding was further confirmed by the ^{14}C measurement of OC and EC in two merged samples selected from a successive synoptic process. The ^{14}C results indicated that biogenic and biomass burning emission contributed 59% and 52% to OC and EC concentrations, respectively, when air masses originated from the Shandong Peninsula, and the contributions fell to 46% and 38%, respectively, when the prevailing wind changed and came from the BTH region. The minimum deviation of the source apportionments from PMF results and ^{14}C measurement was adopted as the optimal choice of the model exercises. Here, two minor overestimations with the same range (3%) suggested that the PMF results provided a reasonable source apportionment of regional $PM_{2.5}$ in this study. Based on the PMF results, eight main sources were identified; of these, coal combustion, biomass burning, and vehicle emission were the largest contributors of $PM_{2.5}$, accounting for 29.6%, 19.3% and 15.8%, respectively. Compared with overall source apportionment, the contributions of vehicle emission, mineral dust and coal combustion, biomass burning increased when air masses came from the BTH region, the Mongolia, and the Shandong Peninsula, respectively. Since coal combustion and vehicle emission have been considered the leading emission sectors to be controlled for improving air quality by the government, biomass burning emission was highlighted in the present study.

Keywords: Source apportionment, PMF, ^{14}C measurement, $PM_{2.5}$

1 Introduction

In recent years, air pollution has become a top environmental issue in China, and the main concern is fine particulate matter less than 2.5 micrometers in diameter ($PM_{2.5}$) (Huang et al., 2014; Sheehan et al., 2014). Fine particulate aerosols have a strong adverse effect on human health, visibility, and directly or indirectly affect weather and climate (Pui et al., 2014). The negative effects on public health, including damage to the respiratory and cardiovascular systems, the blood vessels of the brain, and the nervous system, have triggered both public alarm and official concern in China (Kessler, 2014). In response to this great concern, the Chinese government has introduced the Action Plan for Air Pollution Prevention and Control (2013–17), which aims at marked improvements in air quality until 2017. In the plan, the most severe regulation for improvement is a reduction of 25% in the annual average concentrations of $PM_{2.5}$ by 2017 (Chinese-State-Council, 2013). It has been applied in North China because the region has become the most severely polluted area in China, characterized by increasingly frequent haze events and regional expansions of extreme air pollution (Hu et al., 2015; Boynard et al., 2014).

The key point in reducing $PM_{2.5}$ concentrations is to control its sources. Reliable source identification and quantification are essential for the development of effective political abatement strategies (Balachandran et al., 2013). However, the sources of $PM_{2.5}$ typically emit a mixture of pollutants, including gas and particle phases, which mix further in the atmosphere and can undergo chemical transformations prior to impacting a specific receptor site, making it difficult to quantify the impacts (Balachandran et al., 2013). This encourages researchers to use more techniques to quantify the contribution of individual sources to $PM_{2.5}$ concentrations, such as the Positive Matrix Factorization (PMF) (Paatero and Tapper, 1994), Chemical Mass Balance (CMB) (Chow and Watson, 2002), organic tracers (Ding et al., 2013), and stable carbon isotopes (Cao et al., 2011). However, these different approaches often result in source contributions that can differ in magnitude and/or are poorly correlated, and the most reliable one cannot be determined (Balachandran et al., 2013). Radiocarbon (^{14}C) measurements provide a powerful tool to unambiguously determine fossil and non-fossil sources of carbonaceous particles, and the method has been used in source apportionment of carbonaceous aerosols in China (Zhang et al., 2015; Liu et al., 2013; Liu et al., 2014). The underlying principle of ^{14}C measurements is that the radioisotope has become extinct in fossil fuel carbon due to its age (half-life 5730 years), while its contemporary level in non-fossil carbon sources

is relatively constant (Szidat, 2009; Szidat et al., 2004). This method provides a chance to more reliably source apportion $PM_{2.5}$ by linking with other methods, although it focuses only on carbonaceous aerosols.

In the present study, a more reliable source apportionment of $PM_{2.5}$ at a regional background site in North China during winter was provided using PMF simulation, in which the source contribution of carbonaceous species was confirmed by the ^{14}C measurement. The effort is vital for the development of efficient mediation policies to achieve improvement in air quality in North China because regional source apportionment cannot be replaced by those extensively focused on the metropolitan areas such as Beijing (Zhang et al., 2013), Tianjin (Gu et al., 2011), Jinan (Gu et al., 2014), and others within North China. Thus, we collected continuous aerosol samples on Qimu Island during winter to apportion $PM_{2.5}$ sources. The objectives of this study are (1) to determine the concentration burden and the chemical composition of $PM_{2.5}$, (2) to distinguish the source signals based on the chemical composition grouped according to the trajectory clusters, and (3) to apportion $PM_{2.5}$ sources using the PMF model linked with ^{14}C measurement.

2 Materials and methods

2.1 Sampling site and sample collection

The sampling campaign was conducted from January 3 to February 11, 2014, at the Longkou Environmental Monitoring Station of the State Ocean Administration of China (37°41′N, 120°16′E), on Qimu Island. The island extends to the Bohai Sea westwards, and is surrounded by sea on its other three sides, as shown in Fig. 1. The sampling site is located approximately 15 km northwest of the Longkou urban district and 300 km southeast of the Beijing-Tianjin-Hebei (BTH) region. Longkou city is closest to the sampling site, and emissions from the city can be considered the primary local sources.

A total of 76 $PM_{2.5}$ samples were collected continuously on quartz fiber filters (Whatman, QM-A, 20.3 × 25.4 cm^2, heated at 450 ℃ for 6 h before use) using a Tisch high volume sampler at a flow rate of 1.13 m^3 min^{-1} during the sampling period. The duration for each sample was 12 h, from 06:00–18:00 and from 18:00–06:00 (local time) the next day. Before and after each sample, quartz fiber filters were subjected to 24 h equilibration at 25 ± 1 ^oC temperature and 50 ± 2% relative humidity, and were then analyzed gravimetrically using a Sartorius MC5 electronic microbalance (Zhang et al., 2015; Liu et al., 2013; Huang et al., 2014). Each filter was weighed at least three times.

Acceptable difference among the repetitions was less than 10 μg for a blank filter and less than 20 μg for a sampled filter. After weighing, loaded filters were stored in a refrigerator at -20 ℃ until chemical analysis. In addition, field blank filters were collected to subtract possible contamination occurring during or after sampling.

2.2 Chemical analysis

2.2.1 OC and EC

Organic carbon (OC) and elemental carbon (EC) were analyzed by a Desert Research Institute (DRI) Model 2001 Carbon analyzer (Atmoslytic Inc., Calabasas, CA) following the Interagency Monitoring of Protected Visual Environment (IMPROVE_A) thermal/optical reflectance (TOR) protocol (Chow et al., 2007). A punch of 0.544 cm^2 from each quartz filter was heated to produce four fractions (OC1, OC2, OC3 and OC4) in four temperature steps (140, 280, 480, 580 ℃) under a non-oxidizing helium atmosphere and then in 2% O_2/98% He atmosphere at 580 ℃ (EC1), 740 ℃ (EC2), and 840 ℃ (EC3) for the EC fractions. At the same time, pyrolyzed organic carbon (POC) was produced in the inert atmosphere, which decreased the reflected light to correct for charred OC. The concentrations of OC and EC were obtained according to the IMPROVE protocol, OC = OC1 + OC2 + OC3 + OC4 + POC and EC = EC1 + EC2 +EC3 – POC. The detection limits of the method for OC and EC were 0.82 and 0.20 μg cm^{-2}, respectively. In addition, blank filters and replicate samples were examined simultaneously after analyzing a batch of 10 samples to obtain inherent OC and EC concentrations on the filters and to evaluate measurement accuracy, respectively. In this study, the contributions of OC and EC from blank filters were < 3.5 and 0.6% of their respective average concentrations. The uncertainties of OC (5.6%) and EC (5.5%) were calculated from the replicate measurements.

2.2.2 Water-soluble ions and metal elements

Two 47 mm diameter punches were cut off from each quartz fiber filter, one of which was subjected to Milli-Q water extraction for ionic measurement, and the other underwent induced acid digestion for elemental measurement. The concentrations of water soluble ions (Na^+, NH_4^+, K^+, Mg^{2+}, Ca^{2+}, Cl^-, NO_3^- and SO_4^{2-}) were determined by ion chromatograph (Dionex ICS3000, Dionex Ltd., America) based on the analysis method (Shahsavani et al., 2012). The concentrations of metal elements (including Ti, V, Mn, Fe, Co, Ni, Cu, Zn, As, Cd and Pb) were estimated via inductively coupled plasma mass spectrometry (ICP-MS of ELAN DRCII type, Perkin Elmer Ltd., Hong Kong)

following the previous method (Wang et al., 2006). The detection limit of water-soluble ions was 10 ng ml^{-1} with error < 5%, and 1 ml RbBr of 200 ppm was put in the solution as an internal standard before analysis. The resolution of ICP-MS ranged from 0.3 to 3.0 amu with a detection limit < 0.01 ng/ml, and error < 5%. Five ppb elemental Indium (In) was put in the solution before analysis as an internal standard.

2.2.3 ^{14}C measurement

To achieve more ^{14}C information on carbonaceous fractions in $PM_{2.5}$, OC was split into water-soluble organic carbon (WSOC) and water-insoluble organic carbon (WIOC) fractions. WSOC was extracted from a punch filter by Milli-Q water as described in a previous study (Zhang et al., 2014c), and was quantified as total dissolved organic carbon in solution by a total organic carbon (TOC) analyzer (Shimadzu TOC-VCPH, Japan). WIOC was quantified by OC given by the TOR protocol subtracting WSOC. The uncertainties of WSOC calculated from four time measurements were 6.7% for M1 and 5.3% for M2, while the uncertainties of WIOC were 8.7% and 7.7%, in sequence, estimated by error propagation formulas.

^{14}C measurement of WSOC, WIOC and EC was performed using the OC/EC separation system (Liu et al., 2014). Briefly, the extracted Milli-Q water was freeze-dried, and the residue was re-dissolved and transferred to a pre-combusted quartz tube. Then the quartz tube was combusted at 850 ℃ and WSOC was converted into CO_2. The extracted filters were isolated at 340 ℃ for 15 min for WIOC, after a flash heating of 650 ℃ for 45 s to minimize charring. After separation, the filters were heated at 375 ℃ for 4 h to remove charring, and then oxidized under a stream of pure oxygen at 650 ℃ for 10 min to analyze the EC fraction. Finally, the corresponding evolving CO_2 (WSOC, WIOC and EC) was cryo-trapped and reduced to graphite at 600 ℃ for accelerator mass spectrometry (AMS) target preparation (Xu et al., 2007; Zhang et al., 2010; Wacker et al., 2013). The preparation of graphite targets for AMS analysis was performed using the graphitization line at the Guangzhou Institute of Geochemistry, CAS. The ratios of $^{14}C/^{12}C$ in the graphite samples were determined through a NEC compact AMS at Peking University. In this study, the isolated carbon amounts were typically in the range of 120-280 μg, depending on the samples. The WSOC and WIOC in the blank samples only accounted for 1.94% and 1.15%, respectively, of the average value of M1 and M2, and EC was not found in the blank samples. Thus, the blank interference for the

fractions of modern carbon (f_m) of M1 and M2 in the ^{14}C measurement was very small and was ignored in this study. M1 and M2 are two combined samples for ^{14}C measurement, as elaborated later.

Finally, in order to compensate for the excess ^{14}C caused by nuclear bomb testing in the 1950s and 1960s, the f_m given by AMS was further converted into the fraction of contemporary carbon (f_c). The f_c values in the samples were defined as $f_c = f_m/1.10$ for EC, $f_c = f_m/1.06$ for OC, and the fraction of fossil (f_f) was defined as $f_f = 1 - f_c$ (Zong et al., 2015).

2.3 Data analysis methods

The hybrid single-particle Lagrangian integrated trajectory (HYSPLIT) model was used to generate 48-h backward trajectories with 12 h intervals. The HYSPLIT model is available on the National Oceanic and Atmospheric Administration Air Resource Laboratory website (www.arl.noaa.gov/ready/hysplit4.html). The trajectories were calculated for air masses starting from the sampling site at 500 m above ground level. A total of 152 trajectories were generated and these trajectories were bunched into three clusters by the clustering function in the HYSPLIT model. Air masses from the BTH region, the Mongolia and the Shandong Peninsula were defined as clusters from 1 to 3, respectively, as shown in Fig. 1. The observed chemical components of $PM_{2.5}$ from the three clusters were compared with each other to assess their potential sources.

PMF v5.0 was utilized to apportion $PM_{2.5}$ sources, which is available at the US EPA website: www.epa.gov/air-research/positive-matrix-factorization-model-environmental-data-analyses. PMF is a multivariate factor analysis tool, which assumes that concentrations at a receptor site are supported by linear combinations of different source emissions. Thus, measured mass concentrations of selected species can be mostly expressed as (Paatero et al., 2014):

$$x_{ij} = \sum_{k=1}^{p} g_{ik} f_{kj} + e_{ij} \quad (1)$$

where x_{ij} is the measured concentration of the j^{th} species in the i^{th} sample, f_{kj} is the profile of j^{th} chemical species emitted by the k^{th} source, g_{ik} is the amount of mass contributed by k^{th} source to the i^{th} sample, and e_{ij} is the residual for each samples/species. The matrices of g and f are determined by minimizing an objective function (Paatero et al., 2014).

To further confirm $PM_{2.5}$ sources apportioned by the PMF model, the source contributions of

OC and EC were examined by ^{14}C measurement. The modeled source contributions were merged into two groups according to fossil and contemporary carbon sources. Then the contribution fractions of fossil or contemporary carbon sources to OC and EC could be compared with the ^{14}C measurement for specified samples as:

$$R_{ij} = \sum_{k=1}^{n} g_{ik} f_{kj} \Big/ \sum_{k=1}^{p} g_{ik} f_{kj} \quad (2)$$

where R is the contribution fraction, and matrices of g and f are the same as in eqn(1). The subscript i is a specified sample, j is OC or EC species. n is the number of fossil or contemporary carbon sources, and p is the number of all sources. The minimum deviation of $PM_{2.5}$ source contributions apportioned by the PMF exercises and ^{14}C measurements was used to determine the final model scenario. The model results were treated as providing a more reliable solution for the source apportionment.

2.4 Principle of samples selected for ^{14}C analysis

The comparison of OC and EC focused on cluster 1 and cluster 3 because most species of $PM_{2.5}$ in these two clusters were statistically greater than in cluster 2, as elaborated later. To better achieve the comparison using a few samples for ^{14}C analysis due to its extensive cost, the representative capacity of all samples in the two clusters was examined thoroughly. It is expected that PMF can better interpret those data close to the average condition of each chemical species, since the method utilizes error-minimizing estimates to decompose a matrix of sample data into two matrices under strict non-negativity constraints for the factors (Paatero et al., 2014). Therefore, OC and EC concentrations, and ratios of $OC/PM_{2.5}$ and $EC/PM_{2.5}$ of each sample, were compared with those in the corresponding cluster by mean test.

Finally, two combined samples were selected from a perfect synoptic process during the sampling period. The synoptic process occurred during January 16th and 18th, 2014. As shown in Fig. 2, the first half of air masses in the synoptic process were derived from the south and passed through the Shandong Peninsula (cluster 3) and the bottom half were from the north and passed over the BTH region (cluster 1). Thus, two samples collected continually from 06:00 to 18:00, January 16th and from 18:00 to 06:00 the next day in the first half of the synoptic process were merged into one sample (M1) for the ^{14}C analysis. Similarly, other two samples collected continually from 18:00 to

6:00, January 17th and from 06:00 to 18:00 in the next day were combined into the other sample (M2). M1 reflected the signal of air masses coming from the Shandong peninsula, while M2 showed the pattern of air masses from the BTH region. Mean test showed that except for a significant high ratio of EC/$PM_{2.5}$, the OC and EC concentrations and the OC/$PM_{2.5}$ ratio of M2 were negligibly different from cluster 1, at a 95% significance level, indicating its perfect representative capability for further carbonaceous analysis. However, M1 was not ideal because only ratios of OC/$PM_{2.5}$ and EC/$PM_{2.5}$ had no statistical difference, OC and EC concentrations were significantly higher than that in the cluster 3 at the same significance level. Even so, the samples were still considered for ^{14}C analysis because they were from a faultless synoptic process during the sampling period. Continuous samples were more dramatic than insular samples. In addition, the insignificant difference of the ratios of OC/$PM_{2.5}$ and EC/$PM_{2.5}$ assured the validity for $PM_{2.5}$ source assessment, which was more important than concentration in this study.

3 Results and discussion

3.1 General characteristics of $PM_{2.5}$ and chemical components

Table 1 lists a statistical summary of the concentrations of $PM_{2.5}$, water-soluble ions, carbonaceous species and metal elements during the sampling period. As shown, the mean concentration of $PM_{2.5}$ was 77.6 ± 59.3 μg m^{-3}, which was more than two times higher than the grade I national standards (35 μg m^{-3}, Ministry of Environmental Protection of China: GB 3095-2012, www.zhb.gov.cn, 2012-02-29). Although the level of $PM_{2.5}$ concentration on Qimu Island was higher than the national standard, it was much lower than that observed in winter in the megacities of North China, such as in Beijing (208 μg m^{-3} of $PM_{2.1}$ in 2013) (Tian et al., 2014) and Tianjin (221 μg m^{-3} in 2013) (Han et al., 2014).

For $PM_{2.5}$ components, water-soluble inorganic species (WSIS) were the dominant species, accounting for 37 ± 16 % of $PM_{2.5}$ mass concentrations. Among the ions, SO_4^{2-} ranked the highest with a mean concentration of 14.2 ± 18.0 μg m^{-3}, followed by NO_3^- (11.9 ± 16.4 μg m^{-3}) and NH_4^+ (3.11 ± 2.14 μg m^{-3}). The sum of the three secondary inorganic aerosols constituted the majority (81 ± 12 %) of the total WSIS concentrations. In addition, the average concentrations of OC and EC were 6.85 ± 4.81 and 4.90 ± 4.11 μg m^{-3}, accounting for 9.2 ± 2.1 % and 6.4 ± 1.8 % of the $PM_{2.5}$ concentrations, respectively. Total concentrations of analyzed metal elements were 665 ± 472 ng m^{-3}, accounting for 0.93 ± 0.50 % of the $PM_{2.5}$ mass concentration. Among the measured metal elements,

the concentration of Fe (408 ± 285 ng m^{-3}) was the highest, followed by Zn (107 ± 142 ng m^{-3}), and Pb (88.4 ± 85.7 ng m^{-3}).

The relative contribution of SO_4^{2-}, NO_3^-, and NH_4^+ to the $PM_{2.5}$ at the sampling site was clearly higher than in the cities, such as Beijing and Tianjin, within North China, while the organic matter was clearly lower. The high contributions of SO_4^{2-}, NO_3^-, and NH_4^+ agree with regional scale emissions of their precursors in North China, as it has been reported that SO_2, NO_x, and NH_3 emissions were approximately 10, 5, and 5 times higher compared to OC in the region, respectively (Zhao et al., 2012). This finding was also in agreement with results measured at Changdao Island (Feng et al., 2012). The island, located at the demarcation line between the Bohai Sea and the Yellow Sea, is a resort with little industry approximately 7 km north of the Shandong Peninsula (Feng et al., 2012). Measurements at the island were interpreted as showing patterns of atmospheric outflow and regional pollution in North China (Feng et al., 2012; Feng et al., 2007). It suggested that our measurements also provide a regional signal of $PM_{2.5}$ pollution in North China. Furthermore, SO_4^{2-} was the largest contributor of $PM_{2.5}$, and the highest contributor is usually regarded as a regional pollution signal in winter. This is because during low temperature conditions in $PM_{2.5}$ source areas there is a lack of a fast conversion rate of SO_2 to SO_4^{2-} in clouds or aerosol droplets and oxidation reactions via OH free radicals (Hu et al., 2015). Thus, our measurement largely reflected a pollution pattern on a regional scale, rather than just in source areas.

3.2 Source signals based on cluster analysis

As shown in Fig. 1, the 48-h back trajectory clusters indicate that more than half of the air masses (54%) during the sampling period were from the BTH region (cluster 1), followed by the air masses from Mongolia (35%, cluster 2). Air masses of these two types traveled about 200 and 250 km, respectively, over the Bohai Sea before arriving at the sampling site. Thus, the atmospheric pollutants carried by the two kinds of air masses were mixed well during transport, creating regional pollution signals. Only a small part of the air masses (11%) were from the Shandong Peninsula (cluster 3), potentially reflecting a mixed contribution of local and regional sources from south area of the sampling site. In addition, only one trajectory in cluster 3 passed the urban area of Longkou, when measured $PM_{2.5}$ concentration was 95.3 μg m^{-3}. This level was lower than the average of $PM_{2.5}$ concentrations in cluster 3, listed in Table 2, indicating minor contribution of local source emissions. To reveal the pollution patterns and source signals of $PM_{2.5}$ carried by air masses from the three

different regions, chemical species of $PM_{2.5}$ were grouped according to the three trajectory clusters, as listed in Table 2.

Generally, mean test showed that the concentration levels and most abundant species types of $PM_{2.5}$ in clusters 1 and 3 are both insignificantly different ($p > 0.05$) and statistically higher than in cluster 2 ($p < 0.01$), as shown in Table 2. The patterns observed are consistent with the spatial distributions of their emissions and concentrations in North China; as reported, there are stronger emissions and more serious pollution in the BTH region and Shandong Province than in Inner Mongolia and Liaoning (Zhao et al., 2012; Yang et al., 2011). Compared with Shandong Peninsula, the pollution in BTH region may be more serious because it travels much longer distances to the sampling site, yet $PM_{2.5}$ concentrations attributed to the two areas are insignificantly different. In addition, the mean wind speed of cluster 2 was 7.60 m s^{-1}, which was markedly higher than that of cluster 1 (4.79 m s^{-1}) and cluster 3 (4.86 m s^{-1}). Wind speeds were determined by averaging hourly moving distances of air masses during a 48 h period. The higher wind speed of cluster 2 likely partly contributes to the lower $PM_{2.5}$ level at sampling site, since high wind speed could provide favorable diffusion conditions for atmospheric pollutants.

Some anomalies compared with previous discussion provided different source signals amongst the clusters. For instance, K^+ concentration was significantly higher in cluster 3 than in cluster 1, while the titanium (Ti) concentration was obviously lower. This reflects relatively high emissions of K^+ in the Shandong Peninsula and Ti in the BTH region from both natural sources and anthropogenic activities. Likewise, the concentration of Na^+ in cluster 2 was markedly higher than in clusters 1 and 3, showing the large contribution of sea salt particles generated by sea spray under high wind speed to cluster 2 $PM_{2.5}$ concentrations. This suggested that sea salt sources should not be ignored in this study, due the proximity of the sampling site to the Bohai Sea.

Sea salt emissions are comprised of Cl^-, SO_4^{2-}, Na^+, K^+, Mg^{2+} and Ca^{2+} (Ni et al., 2013). The amounts of different chemical species in sea salt emissions can be determined from using Na^+ as the tracer of sea salt; the amounts of these species from non-sea salt (nss-) emissions can be expressed as:

$$nss\text{-}x = x - [Na^+] \times a \quad (3)$$

where x indicates the Cl^-, SO_4^{2-}, K^+, Mg^{2+} and Ca^{2+} concentrations, and a is the typical equivalent concentration ratio of the corresponding species to Na^+ in average seawater: Cl^-/Na^+ (1.80), SO_4^{2-}/Na^+ (0.25), K^+/Na^+ (0.036), Mg^{2+}/Na^+ (0.12) and Ca^{2+}/Na^+ (0.038) (Ni et al., 2013). If the calculated concentration of non-sea salt chemical species is negative, then no excess species exist. According to the calculation, for corresponding total chemical concentration levels grouped in clusters from 1 to 3, nss-Cl^- accounted for 55 ± 29%, 19 ± 24% and 77 ± 10% of total Cl^-; nss-SO_4^{2-} accounted for 99 ± 2%, 95 ± 4% and 99 ± 0.3% of total SO_4^{2-}; nss-K^+ accounted for 98 ± 3%, 89 ± 9% and 99 ± 0.3% of total K^+; nss-Ca^{2+} accounted for 95 ± 4%, 91 ± 10% and 96 ± 3% of total Ca^{2+}. Thus, marked contributions of nss-emission sources to chemical concentrations at all three clusters were found. However, these values may be underestimated, since total Na^+ concentrations do not necessarily originate from sea salt alone, but could partially come from dust and burning sources (Zhang et al., 2013). In addition, the loss of Cl^- particles due to a chloride depletion mechanism further supports the underestimation of Cl^-. The contributions of nss-sources were lower in cluster 2 than in clusters 1 and 3, which was attributed to high emissions of sea spray coupled with high wind speed in cluster 2. Generally, K^+ is often used as a tracer for biomass burning. The high K^+ concentration and the largest contribution of nss-K^+ in cluster 3 indicated clearly high emissions associated closely with agricultural burning in the Shandong Peninsula. This finding agreed with the fact that Shandong is the largest producer of crop residues in North China (Zhao et al., 2012), and biomass burning is an important source of inorganic and organic aerosols in the Bohai sea atmosphere (Feng et al., 2012; Wang et al., 2014). The contribution of nss-Mg^{2+} to total magnesium concentration was less than 4% for the all clusters, indicating the species came mostly from sea salt emission. The mass ratio of Mg^{2+} to Na^+ was 0.07 ± 0.06, 0.06 ± 0.03 and 0.06 ± 0.03 for clusters from 1 to 3, respectively. The ratios were less than 0.23, also demonstrating that Mg^{2+} mostly came from sea salt source (Zhang et al., 2013).

The ratios of OC/EC and NO_3^-/nss-SO_4^{2-} were used as tracers to assess source signals of the three clusters. Low temperature burning, such as agricultural residue burning, emits more OC compared with high temperature burning, e.g. vehicle exhaust. Thus, the ratio of OC to EC is often used to evaluate relative contributions of low and high temperature burning emission (Zhao et al., 2012). The OC/EC ratios were 1.41 ± 0.30, 1.47 ± 0.29 and 2.14 ± 0.50 for clusters 1 to 3, respectively. Mean test showed that the difference between cluster 1 and cluster 2 ratios were

insignificant at a 95% confidence level, and both clusters 1 and 2 ratios were statistically lower compared with that of cluster 3, at the same confidence level. This suggests that low temperature burning clearly contributed to emission in cluster 3, while high temperature burning emission was more distinct in clusters 1 and 2. Furthermore, mobile sources, such as vehicles, exhaust more NO_x than SO_2, while stationary sources, such as coal-fired power plants, emit more SO_2 than NO_x (Wang et al., 2005). These two precursors convert into SO_4^{2-} and NO_3^- in the atmosphere, and the two type sources show different ratios of NO_3^-/SO_4^{2-}. Hence, this ratio is often used as an indicator of the relative importance of mobile vs. stationary sources of sulfur and nitrogen in the atmosphere (Zhao et al., 2013; Liu et al., 2014). In this study, after deducting the contribution of sea salt to SO_4^{2-}, the mean ratios of NO_3^-/nss-SO_4^{2-} were 0.96 ± 0.31, 0.47 ± 0.24 and 0.64 ± 0.14 for clusters 1 to 3, respectively. Mean test showed that the three cluster ratios exhibit significant differences from each other at a 95% confidence level. The highest ratio in cluster 1 suggests that amongst the three regions, mobile sources are the most important contributors of in the BTH region, followed by Shandong Peninsula (cluster 3). The ratio of NO_3^-/nss-SO_4^{2-} in cluster 1 was within the range of those found in large cities, such as Beijing (1.20), Tianjin (0.73), and Shijiazhuang (0.76), the capital of Hebei province (Zhao et al., 2013), reflecting a hybrid contribution from the BTH region. The value in cluster 2 was slightly lower than that in winter in Chengde (0.55), one city located in the northern mountainous area of Hebei Province (Zhao et al., 2013). It indicated more obvious contribution of stationary source emissions in areas such as eastern Inner Mongolia and the west part of Liaoning, than from the BTH region and the Shandong Peninsula. These stationary source emissions are possibly associated with coal combustion because of the lower OC/EC ratio in cluster 2 compared to cluster 3.

3.3 Source apportionment of carbonaceous $PM_{2.5}$

The cluster analysis clearly indicated that $PM_{2.5}$ concentrations increased significantly when air masses came from the BTH region and the Shandong Peninsula during the sampling period. The chemical species in $PM_{2.5}$ from the BTH region possessed more marked signals of high temperature burning and mobile sources, while those from the Shandong Peninsula had more obvious patterns of low temperature burning and stationary sources.

Table 3 lists the concentrations and contemporary carbon fractions of OC, WSOC, WIOC and EC of the two combined samples, which were selected via a perfect synoptic process during the

sampling period. The fraction of OC was yielded by the average weights of concentrations of WSOC and WIOC fractions. It can be expressed as:

$$f_c(\mathrm{OC}) = [f_c(\mathrm{WSOC}) \times c(\mathrm{WSOC}) + f_c(\mathrm{WIOC}) \times c(\mathrm{WIOC})]/[c(\mathrm{WSOC}) + c(\mathrm{WIOC})] \quad (4)$$

where f_c(OC), f_c(WSOC) and f_c(WIOC) are the contemporary carbon fractions of OC, WSOC and WIOC, and c(WSOC)and c(WIOC) are the concentrations of WSOC and WIOC, respectively. Generally, WSOC is mainly associated with biomass burning and secondary formation (Du et al., 2014), while OC directly emitted from the combustion of fossil fuel is mostly water insoluble (Weber et al., 2007). During the earlier stage of the synoptic process, the concentrations of WSOC and WIOC were 6.4 μg m^{-3} and 6.3 μg m^{-3}, respectively. Later on, the concentrations of the two carbonaceous fractions fell to 3.7 μg m^{-3} and 5.3 μg m^{-3}, respectively, after the shift of the dominant wind direction from southerly to northwesterly, as shown in Fig. 2. The fraction of WSOC to OC decreased from 50% to 41% and the WIOC fraction increased from 50% to 59% before and after the shift of the dominant wind direction. This suggested that the contribution of fossil fuel combustion was more obvious in the BTH region than in the Shandong Peninsula. The contemporary carbon fractions of WSOC and WIOC decreased from 0.59 to 0.49 and from 0.60 to 0.43, respectively, which indicated a decrease in the impact of biogenic and biomass burning emission and an increase in contribution of fossil fuel combustion to the two OC fractions after the shift of the prevailing wind. After the weighted average of the WSOC and WIOC fractions, the f_c(OC) values were 0.59 and 0.46 for the M1 and M2 samples, respectively. Together with f_c (EC), we determined that biogenic and biomass burning emission contributed 59% of OC and 52% of EC concentrations, respectively, when air masses were from the Shandong Peninsula. After the change of wind direction, the contribution of biogenic and biomass burning emission fell to 46% for OC and 38% for EC, respectively, which suggested that fossil fuel combustion contributed a dominant portion of the carbonaceous aerosols from the BTH region.

The synoptic process clearly showed a shift of the dominant wind from southerly to northwesterly, namely from the Shandong Peninsula to the BTH region. Meanwhile, the pattern of biogenic and biomass burning emission became more and more weak, and the signal of fossil fuel combustion became more and more obvious. This was in agreement with our previous discussion. For instance, emissions in the BTH region exhibited more signals of high temperature burning and vehicle exhaust. It was characterized by the lower ratio of OC/EC (1.41 ± 0.30), the higher ratio of

NO_3^-/nss-SO_4^{2-} (0.96 ± 0.31), and the relatively lower concentration of nss-K^+ compared with those in the Shandong Peninsula (2.14 ± 0.50 for OC/EC ratio, 0.64 ± 0.14 for NO_3^-/nss-SO_4^{2-} ratio). The contribution of the biogenic and biomass burning emission to carbonaceous aerosols in the Shandong Peninsula was still significant, which has often been mentioned in previous studies (Feng et al., 2012; Zong et al., 2015; Wang et al., 2014), although there was great combustion of fossil fuel (e.g., coal) for not only industrial activity but also heating in winter.

3.4 Source apportionment of $PM_{2.5}$

The EPA PMF 5.0 model was used together with a date set of 76×22 (76 samples with 22 species) to further quantitatively estimate the source contributions of $PM_{2.5}$. After iterative testing from 5 to 15 factors in model exercises, we found the minimum deviation of the source apportionments of OC and EC between the results from ^{14}C measurement and a PMF model scenario with an F_{peak} value of 0 and the lowest Q values (6245).

Based on PMF modeling results, eight source factors were identified, as shown in Fig. 3. Traffic emission has attracted considerable concern in the megacities of China (e.g., Beijing and Shanghai) due to the remarkable growth of vehicle numbers in China. In Beijing in 2012, on-road vehicles were estimated to be the largest local emission source and contributed 22% of $PM_{2.5}$, including primary and secondary fine particles and excluding vehicle-induced road dust (Zhang et al., 2014b). The first source factor was characterized by high loadings of NO_3^-, SO_4^{2-}, NH_4^+, OC, EC, Zn and Cu, which matched a vehicle emission profile (Zhang et al., 2013). Generally, NO_3^-, SO_4^{2-}, OC and EC are mainly from engine exhaust emissions, and ammonia is from vehicles equipped with three-way catalytic converters. Not only Zn and Cu, but also Pb and Cd are emitted directly bounded particles from exhaust (Zhang et al., 2014b). In addition, the high NO_3^-/SO_4^{2-} ratio of 1.28 calculated by the PMF results suggested high temperature burning and vehicle emissions. This source was the largest contributor of NO_3^-, which contributed 41% during the sampling period. The contribution was higher than 31% of NO_x emitted by traffic sectors in North China in 2003, an expected increase of the contribution due to the rapid rise of vehicles in North China in recent years (Shi et al., 2014b). This factor was the prevalent anthropogenic $PM_{2.5}$ source in North China, with an average contribution of 16% during the sampling period. The contribution was lower than that in Beijing (Zhang et al., 2014b), agreeing with the regional contribution characteristic in our study, rather than ones in large cities, where a large number of vehicles run. The second factor consisted of mineral dust elements,

such as Mn, Fe and Co, and chemical species from human activities, such as Zn and EC, showing a mixed pattern of natural and anthropogenic emissions. Vehicle emission is an important source of atmospheric Zn pollution because it can be emitted from direct exhaust, lubricating oil additives, tire and brake abrasion, wearing and corrosion from anticorrosion galvanized automobile sheet, and re-entrainment dust enriched with Zn (Duan and Tan, 2013). Thus, the source factor was identified as traffic dust under the relative high contribution of vehicle emission to $PM_{2.5}$ concentration.

The third source factor was ship emissions, typically characterized by high proportions of Ni and V, and a high V/Ni ratio. High loading of these two metals is typically associated with emissions from residual oil, probably derived from shipping activities and some industrial processes (Pey et al., 2013). In addition, a V/Ni ratio of more than 0.7 is always considered a sign of $PM_{2.5}$ influenced by shipping emissions (Zhang et al., 2014a). The average ratio of V/Ni from the measured data was 0.93 $\pm$0.46, indicating an obvious contribution of shipping emission. The average ratio of V/Ni calculated from the PMF source profile was 1.02, which was the second highest value amongst those derived from the eight sources. The highest value of 1.29 was for the mineral dust source, which agreed with a high ratio of 3.06 for soil background concentrations of the two metals in mainland China (Pan et al., 2013).

The fourth factor showed high loadings of Cu, Zn, As, Cd and Pb, which were treated as signals of industrial processes. Emissions from the iron and steel industry are possibly important amongst those industrial processes for two reasons. One is that the sintering process in the iron and steel industries emits large amounts of Pb, Hg, Zn and other heavy metal pollutants, and other processes such as ironmaking and steelmaking also emit fugitive dust containing high concentrations of heavy metals (Duan and Tan, 2013). The other reason is the huge scale of steel production in North China. National statistical data shows that China produced approximately half the world's production of crude steel in 2014, and production in the BTH and Shandong were 25.3% and 7.8%, respectively, of the total amount in China, respectively, which is available at the website (http://www.stats.gov.cn/tjsj/ndsj/). Thus, iron and steel industries are likely the main atmospheric sources of the metal elements in this study. In addition, the contribution of the source to SO_4^{2-} was 12%, which was similar to previously reported contributions of industrial processes to the amount of sulfur dioxide (15%) (Zhao et al., 2012).

The fifth source factor was biomass burning, characterized by high concentrations of K^+, OC,

EC and NH_4^+, which have been used extensively as tracers of biomass-burning aerosols (Zhou et al., 2015; Tao et al., 2014). The contribution of this source was significantly higher in cluster 3 than in clusters 1 and 2, as listed in Table 4. Results agreed with more biomass burning emission in the Shandong Peninsula, characterized by rich K^+ and the high OC/EC ratio. The average ratio of OC to EC from this source was also the highest (1.84) amongst the eight identified sources (0.23-1.84) calculated by the PMF modeling.

The sixth source factor was mineral dust, characterized typically by crustal elements, such as Ca^{2+}, Ti and Fe, which are often used as markers of soil dust (Zhang et al., 2013). The contribution of this source was obviously higher in cluster 2 than that in clusters 1 and 3, corresponding to high wind speed in cluster 2. The average ratio of OC to EC (1.53) from this source was obviously higher than that (0.23) from vehicle dust, possibly suggesting that the source contributed more OC, mainly derived from biogenic dust, such as plant debris.

The seventh source factor was characterized by high loadings of Cl^-, Na^+, OC, EC, SO_4^{2-} Ni and As. Coal combustion is often indicated by elevated Cl^- linked with high Na^+, OC and EC (Zhang et al., 2013). This source was the largest contributor of SO_4^{2-} in the present study, matching with the inventory results in North China (Zhao et al., 2012). In addition, this source was the largest contributor of $PM_{2.5}$, as listed in Table 4, which agreed with the fact that coal combustion is considered the predominant source of fine particle aerosols over China (Pui et al., 2014). High loadings of As and Ni in the factor was also used as a marker for coal-fired power plant emissions (Tan et al., 2016).

The last source factor was sea salt, characterized by high loading of Na^+, Mg^{2+} and Cl^-, which are related to the primary sea-salt aerosols produced by mechanical disruption of the ocean surface. Similarly to the second source (mineral dust), high wind speed in cluster 2 made the contribution of this source in cluster 2 higher than that in clusters 1 and 3. In addition, the higher contribution fractions of Mg^{2+} compared to Cl^- in this source were in agreement with our previous discussion. The concentration ratios of Cl^-/Na^+ and Mg^{2+}/Na^+ calculated from the PMF source profile were 1.79 and 0.11, respectively, similar to the corresponding ratios of the species (1.80 and 0.12, respectively) in average seawater (Ni et al., 2013). The sea salt source contributed 2.53%, 15.2% and 1.93% of OC concentrations in clusters 1 to 3, respectively, but provided no EC contribution in any of the clusters. This indicates the source consists of sea-spray organic aerosols, which were produced by marine

biogenic activities (Wilson et al., 2015).

The contributions of the eight sources to $PM_{2.5}$ are summarized in Table 4. The total and cluster fractional contributions (%) from each source were calculated based on the corresponding sample values simulated by PMF modeling. Amongst the eight sources identified by the PMF modeling, coal combustion, biomass burning and vehicle emissions were the largest contributors of $PM_{2.5}$, which accounted for 29.6%, 19.3% and 15.8%, respectively, during the sampling period. They were followed, in decreasing order, by mineral dust (12.8%), ship emissions (8.95%), sea salt (6.58%), traffic dust (4.24%) and industrial process (2.64%). Generally, the source apportionment profile of $PM_{2.5}$ in cluster 1 was similar to that during the whole sampling period, because the regional scale pollution mainly exhibited a pattern of atmospheric outflow of $PM_{2.5}$ from the BTH region in winter (Feng et al., 2007; Feng et al., 2012). A slight increase in the contribution of vehicle emission in cluster 1 corresponds to the great concern about vehicle emission in megacities in China (Zhang et al., 2014b). The source signals in cluster 2 were obviously different from that in clusters 1 and 3. The strong northwesterly wind in it provided more large scale spatial signals of $PM_{2.5}$ sources, indicating that coal combustion (37.7%) and mineral dust (26.8%) were the largest contributors in north areas of China in winter. The large scale $PM_{2.5}$ pattern linked to coal combustion agreed with the dominant position of coal consumption in Chinese energy structure; coal consumption accounted for 66% of primary energy in China in 2014 by the national bureau of statistics of China (available at http://www.stats.gov.cn/tjsj/ndsj/). Other than industrial consumption, coal is additionally used for residential heating in northern areas of China during winter. Although the household use of coal accounts for a small portion of total coal consumption in China, its release is still a major source of $PM_{2.5}$ in winter (Cao et al., 2012), since household stoves usually run with no or outdated environmental protection equipment. Traffic emission, of much concern in large cities, only contributed a minor part (3.57%) of $PM_{2.5}$ concentrations on a large spatial scale because motor exhaust concentrates mainly in urban areas. In addition, biomass burning emission dominated the $PM_{2.5}$ pollution when air masses came from the Shandong Peninsula. The abundant emission from biomass burning was mainly attributed to residential heating in the cold season.

The contributions of coal combustion, vehicle emission, industrial process, and ship emission derived from the PMF modeling of OC and EC were ranked as fossil fuel combustion for comparison. Sea salt as a marine biogenic source of OC was merged with biomass burning as contemporary

carbon fractions. However, mineral dust and vehicle dust were not considered for this classification, because they originated from hybrid sources of fossil and contemporary carbon emissions. Fig. 4 shows the comparison of the PMF results and the ^{14}C measurement.

As described in section 2.4, M1 represents the air mass from Shandong peninsula, while M2 is on behalf of the air mass from BTH region. In M1, the biogenic and biomass burning emission identified by PMF modeling contributed 52% to OC and 49% to EC concentrations, which were 7 and 3 % below the fractions indicated by ^{14}C measurement, respectively,. The contributions of fossil fuel combustion to OC and EC from the PMF result were both 44%, which is 3 percent over and 4 percent below the corresponding values in the ^{14}C result. Similarly, in M2, the biogenic and biomass burning emission contributed 41% to OC and 33% to EC in the PMF result, 4 and 5 percent below the ^{14}C result, respectively. The contributions of fossil fuel combustion to OC and EC in the PMF result were 52% and 65%, respectively, which were the same percent (3%) below and over the corresponding values in the ^{14}C result. In general, the source contributions merged from the PMF results were lower than those from the ^{14}C measurement. This underestimation may be due to not considering the contributions of mineral dust and vehicle dust because of their hybrid sources. The largest difference between PMF and ^{14}C results was 7%, indicating a minor contribution of the two sources to carbonaceous species in $PM_{2.5}$. The substantial difference was the two overestimations with the same range (3%); one was the contribution of fossil fuel combustion to OC in M1 and the other was the contribution of fossil fuel combustion to EC in M2. The overestimation was attributed to irrelevantly classifying biogenic and biomass burning emission as fossil fuel combustion. In conclusion, the minor irrelevant classification suggested that the PMF result in this study provided a reasonable source apportionment of regional $PM_{2.5}$ in North China in winter.

4 Implications for PM alleviation

According to source apportionment results, coal combustion was the largest contributor of $PM_{2.5}$ in North China during winter, and this source imposed a larger spatial pattern of $PM_{2.5}$ pollution in northern areas of China compared with North China. Therefore, to alleviate overall PM emissions, those generated by coal combustion should be first targeted. The source has been identified as the leading emission sector for controlling the annual $PM_{2.5}$ concentration in the air pollution control program. The contributions of traffic emission and biomass burning to $PM_{2.5}$ concentrations also formed a clear spatial pattern in North China during winter. Vehicle emission contributed

significantly to $PM_{2.5}$ in the BTH region, so for regulations this source should be considered the second major emission sector to control.

Biomass burning emission should be paid close attention to because the emission has been only lightly considered in the control program. Indeed, the first national pollution source survey showed that Shandong province is the largest producer of crop stalks, with a production of 132 million tons in China in 2007 (Compilation Committee of the first China pollution source census, 2011). Of these, about 20 million tons were produced in the Shandong Peninsula (including the cities of Weifang, Yantai, Weihai, Qingdao and Rizhao). Approximately 40% of this production was used as household fuel for cooking and heating in the peninsula countryside. The fraction was significantly higher than in western areas of the Shandong province, such as Zibo (9%) and Jinan (8%), and the fraction of open burning of crop residues in the peninsula (3%). The fraction of biomass open burning in the peninsula was also higher than the average fraction (1.5%) in Shandong province in 2007. Generally, emissions from agricultural field burning are mainly concentrated in the harvest season and contribute significantly to regional haze and smog events in the region, which have attracted special concern (Feng et al., 2012; Zong et al., 2015; Wang et al., 2014). Despite this, open burning emission has been considered only as a minor source sector in the control program. Household emission of agricultural waste, another larger source, are released continuously or semi-continuously, and can also induce $PM_{2.5}$ pollution on a regional scale, which has also been despised or ignored (Zhang and Cao, 2015).

Open burning is not fully controlled in China, although the government has enacted a series of regulations to prohibit field burning since the 1990s and strengthened the force of its supervision recently. The most basic reason for continued burning is the lack of a reasonable alternative to utilize or dispose of huge amounts of agricultural waste each year. In the current scenario, some agricultural wastes are collected and stored as fuel for household cooking and heating, and others are rapidly removed by open burning in fields for the next planting during harvest season. Although farmers know that such use and disposal of agricultural residues are harmful to the environment, they still tend to use agricultural wastes as household fuel and burn wastes in fields, mainly due to the low costs of the methods. A more permanent solution would be to find higher economic value in agricultural wastes via development of renewable techniques. Indeed, agricultural wastes can be utilized to produce many renewable energies, such as biogas, feedstuffs, biochar, bioethanol, and

bio-succinic acid. China has provided relevant energy regulations, legislation, and policy initiatives for rural renewable energy (Li et al., 2015). The government has also encouraged and sustained the development of the renewable energy industry to increase the demand for raw feedstocks. Through these efforts, China has achieved some success in renewable development in rural areas, but these efforts are not an effective solution to the problem of surplus crop waste, because the costs and benefits cannot yet be offset. For instance, Zhangziying, a town located in the eastern area of the Daxing district of Beijing, has developed household biogas and straw gas since the 1980s, but in 2011 renewable energy only made up approximately 10% of household energy consumption, much lower than the fraction of coal (30%) (Li et al., 2015). Before the achievement of high economic value, except for the ban on crop straw burning, the government should compensate farmers to collect crop residues as feedstocks of renewable energy, rather than burning in fields or households (Shi et al., 2014a). The revenue from the subsidy and sale of crop residues could help alleviate economic burdens on farmers, so they can use clean energy, such as electricity, liquefied petroleum gas, biogas, etc., for household consumption (Kung and Zhang, 2015). These efforts will not only significantly improve air quality, but also make famers learn the convenience of clean energy and wake from agricultural residue burning.

5 Conclusions

During the sampling period, the average $PM_{2.5}$ concentration was 77.6 ± 59.3 μg m^{-3}, and SO_4^{2-} concentration was the highest of any constituent, with a mean of 14.2 ± 18.0 μg m^{-3}, followed by NO_3^- (11.9 ± 16.4 μg m^{-3}), OC (6.85 ± 4.81 μg m^{-3}), EC (4.90 ± 4.11 μg m^{-3}), and NH_4^+ (3.11 ± 2.14 μg m^{-3}). The fractions of SO_4^{2-}, NO_3^- and NH_4^+ to $PM_{2.5}$ were obviously higher than those in metropolises (e.g. Beijing and Tianjin) within North China, while fractions of carbonaceous species were markedly lower; these showed regional pollution signals.

More than half of air masses during the sampling period were from the BTH region, followed by air masses from Mongolia (35%) and the Shandong Peninsula (11%). The concentrations of $PM_{2.5}$ and most of the species carried by the air masses from the BTH region and the Shandong Peninsula were comparable ($p > 0.05$), and they occurred in statistically greater concentrations than those carried by the air masses from Mongolia ($p < 0.01$). The $PM_{2.5}$ had an obvious signal of biomass burning emission, characterized by a high OC/EC ratio, low NO_3^-/nss-SO_4^{2-} ratio and high nss-K^+ concentration when air masses came from the Shandong Peninsula. In contrast, the $PM_{2.5}$ carried

from the BTH region showed vehicle emission pattern, characterized by low OC/EC ratio, high NO_3^-/nss-SO_4^{2-} ratio and low nss-K^+ concentration. This finding was confirmed by the ^{14}C measurement of OC and EC in two merged samples selected from a successive synoptic process. The ^{14}C measurement indicated that biogenic and biomass burning emission contributed 59% and 52% of OC and EC concentrations when air masses were from the Shandong Peninsula, and the contributions fell to 46% and 38%, respectively, when the prevailing wind changed and came from the BTH region.

Based on the PMF modeling result, eight main source factors were identified. The source contribution of OC and EC derived from PMF for the two specified samples was compared with that indicated by the ^{14}C assessment. Two minor overestimations with the same range (3%) showed the excellent capacity of the model, suggesting that the PMF result provided a reasonable source apportionment of regional $PM_{2.5}$ in the North China in winter. The PMF results indicated that coal combustion, biomass burning and vehicle emissions were the largest contributors of $PM_{2.5}$, accounting for 29.6%, 19.3% and 15.8% of $PM_{2.5}$, respectively, during the sampling period. Compared with overall source apportionment result, the contribution of vehicle emission increased slightly when air masses came from the BTH region, the fraction of mineral dust and coal combustion rose clearly when air masses with high speed were from Mongolia, and biomass burning became the dominant contributor when air masses were from the Shandong Peninsula. Biomass burning emission was highlighted in the present study, because coal combustion and vehicle emission have already been considered as major emission factors in the government air pollution control program.

Furthermore, the present study proposed that the minimum deviation between the results from PMF model and ^{14}C measurement could be used as a criterion to select a more reliable solution for source apportionment of $PM_{2.5}$. This method can be applied to CMB models or other isotopes (e.g. ^{13}C, ^{15}N and ^{35}S), which will help to improve scientific significance.

Acknowledgment

This work was supported by the CAS Strategic Priority Research Program (Nos. XDA11020402, XDB05030303 and XDB05040503), and the Natural Scientific Foundation of China (Nos. 41471413 and 41373131). The authors gratefully acknowledge the National Oceanic and Atmospheric

Administration's Air Resources Laboratory for providing the HYSPLIT transport model and the READY website (http://www.arl.noaa.gov/ready.html).

Notes

The authors declare no competing financial interest.

Reference

Balachandran, S., Chang, H. H., Pachon, J. E., Holmes, H. A., Mulholland, J. A., and Russell, A. G.: Bayesian-based ensemble source apportionment of $PM_{2.5}$, Environ. Sci. Technol., 47, 13511-13518, doi: 10.1021/es4020647, 2013.

Boynard, A., Clerbaux, C., Clarisse, L., Safieddine, S., Pommier, M., Van Damme, M., Bauduin, S., Oudot, C., Hadji-Lazaro, J., Hurtmans, D., and Coheur, P.-F.: First simultaneous space measurements of atmospheric pollutants in the boundary layer from IASI: A case study in the North China Plain, Geophys. Res. Lett., 41, 645-651, doi: 10.1002/2013gl058333, 2014.

Cao, J.-j., Chow, J. C., Tao, J., Lee, S.-c., Watson, J. G., Ho, K.-f., Wang, G.-h., Zhu, C.-s., and Han, Y.-m.: Stable carbon isotopes in aerosols from Chinese cities: Influence of fossil fuels, Atmos. Environ., 45, 1359-1363, doi: 10.1016/j.atmosenv.2010.10.056, 2011.

Cao, J.-J., Shen, Z.-X., Chow, J. C., Watson, J. G., Lee, S.-C., Tie, X.-X., Ho, K.-F., Wang, G.-H., and Han, Y.-M.: Winter and summer $PM_{2.5}$ chemical compositions in fourteen Chinese cities, J. Air Waste Manage. Assoc., 62, 1214-1226, doi: 10.1080/10962247.2012.701193, 2012.

Chinese-State-Council: Atmospheric Pollution Prevention and Control Action Plan, http://www.gov.cn/zwgk/2013-09/12/content_2486773.htm (in Chinese), access: 12, September, 2013.

Chow, J. C., and Watson, J. G.: Review of $PM_{2.5}$ and PM_{10} apportionment for fossil fuel combustion and other sources by the chemical mass balance receptor model, Energy Fuels, 16, 222-260, doi: 10.1021/ef0101715,

2002.

Chow, J. C., Watson, J. G., Chen, L. W. A., Chang, M. C. O., Robinson, N. F., Trimble, D., and Kohl, S.: The IMPROVE_A temperature protocol for thermal/optical carbon analysis: Maintaining consistency with a long-term database, J. Air Waste Manage. Assoc., 57, 1014-1023, doi: 10.3155/1047-3289.57.9.1014, 2007.

Compilation-Committee-of-the-first-China-pollution-source-census: Dataset of the first China pollution source census, China Environmental Science Press, Beijing, 120 pp., 2011.

Ding, X., Wang, X., Xie, Z., Zhang, Z., and Sun, L.: Impacts of siberian biomass burning on organic aerosols over the north pacific ocean and the arctic: Primary and secondary organic tracers, Environ. Sci. Technol., 47, 3149-3157, doi: 10.1021/es3037093, 2013.

Du, Z., He, K., Cheng, Y., Duan, F., Ma, Y., Liu, J., Zhang, X., Zheng, M., and Weber, R.: A yearlong study of water-soluble organic carbon in Beijing I: Sources and its primary vs. secondary nature, Atmos. Environ., 92, 514-521, doi: 10.1016/j.atmosenv.2014.04.060, 2014.

Duan, J., and Tan, J.: Atmospheric heavy metals and Arsenic in China: Situation, sources and control policies, Atmos. Environ., 74, 93-101, doi: 10.1016/j.atmosenv.2013.03.031, 2013.

Feng, J., Guo, Z., Chan, C. K., and Fang, M.: Properties of organic matter in $PM_{2.5}$ at Changdao Island, China—A rural site in the transport path of the Asian continental outflow, Atmos. Environ., 41, 1924-1935, doi: 10.1016/j.atmosenv.2006.10.064, 2007.

Feng, J., Guo, Z. G., Zhang, T. R., Yao, X. H., Chan, C. K., and Fang, M.: Source and formation of secondary particulate matter in $PM_{2.5}$ in Asian continental outflow, J. Geophys. Res., 117, D03302, doi: 10.1029/2011jd016400, 2012.

Gu, J., Bai, Z., Li, W., Wu, L., Liu, A., Dong, H., and Xie, Y.: Chemical composition of $PM_{2.5}$ during winter in Tianjin, China, Particuology, 9, 215-221, doi: 10.1016/j.partic.2011.03.001, 2011.

Gu, J., Du, S., Han, D., Hou, L., Yi, J., Xu, J., Liu, G., Han, B., Yang, G., and Bai, Z.-P.: Major chemical compositions, possible sources, and mass closure analysis of $PM_{2.5}$ in Jinan, China, Air Qual. Atmos. Health, 7, 251-262, doi: 10.1007/s11869-013-0232-9, 2014.

Han, S.-q., Wu, J.-h., Zhang, Y.-f., Cai, Z.-y., Feng, Y.-c., Yao, Q., Li, X.-j., Liu, Y.-w., and Zhang, M.: Characteristics and formation mechanism of a winter haze–fog episode in Tianjin, China, Atmos. Environ., 98, 323-330, doi: 10.1016/j.atmosenv.2014.08.078, 2014.

Hu, M., Guo, S., Peng, J.-f., and Wu, Z.-j.: Insight into characteristics and sources of $PM_{2.5}$ in the Beijing–Tianjin–Hebei region, China, Natl. Sci. Rev., 2, 257-258, doi: 10.1093/nsr/nwv003, 2015.

Huang, R.-J., Zhang, Y., Bozzetti, C., Ho, K.-F., Cao, J.-J., Han, Y., Daellenbach, K. R., Slowik, J. G., Platt, S. M., Canonaco, F., Zotter, P., Wolf, R., Pieber, S. M., Bruns, E. A., Crippa, M., Ciarelli, G., Piazzalunga, A., Schwikowski, M., Abbaszade, G., Schnelle-Kreis, J., Zimmermann, R., An, Z., Szidat, S., Baltensperger, U., Haddad, I. E., and Prevot, A. S. H.: High secondary aerosol contribution to particulate pollution during haze events in China, Nature, 514, 218–222, doi: 10.1038/nature13774, 2014.

Kessler, R.: Prevention: Air of danger, 509, S62-S63, doi: 10.1038/509S62a, 2014.

Kung, C.-C., and Zhang, N.: Renewable energy from pyrolysis using crops and agricultural residuals: An economic and environmental evaluation, Energy, 90, Part 2, 1532-1544, doi: 10.1016/j.energy.2015.06.114, 2015.

Li, X., Lin, C., Wang, Y., Zhao, L., Duan, N., and Wu, X.: Analysis of rural household energy consumption and renewable energy systems in Zhangziying town of Beijing, Ecol. Modell., 318, 184-193, doi: 10.1016/j.ecolmodel.2015.05.011, 2015.

Liu, D., Li, J., Zhang, Y., Xu, Y., Liu, X., Ding, P., Shen, C., Chen, Y., Tian, C., and Zhang, G.: The use of levoglucosan and radiocarbon for source apportionment of $PM_{2.5}$ carbonaceous aerosols at a background site

in East China, Environ. Sci. Technol., 47, 10454-10461, doi: 10.1021/es401250k, 2013.

Liu, J., Li, J., Zhang, Y., Liu, D., Ding, P., Shen, C., Shen, K., He, Q., Ding, X., Wang, X., Chen, D., Szidat, S., and Zhang, G.: Source apportionment using radiocarbon and organic tracers for $PM_{2.5}$ carbonaceous aerosols in Guangzhou, South China: Contrasting local- and regional-scale haze events, Environ. Sci. Technol., 48, 12002-12011, doi: 10.1021/es503102w, 2014.

Ni, T., Li, P., Han, B., Bai, Z., Ding, X., Wang, Q., Huo, J., and Lu, B.: Spatial and Temporal Variation of Chemical Composition and Mass Closure of Ambient PM_{10} in Tianjin, China, Aerosol Air Qual. Res., 13, 1832-1846, doi: 10.4209/aaqr.2012.10.0283, 2013.

Paatero, P., and Tapper, U.: Positive matrix factorization: A non-negative factor model with optimal utilization of error estimates of data values, Environmetrics, 5, 111-126, doi: 10.1002/env.3170050203, 1994.

Paatero, P., Eberly, S., Brown, S. G., and Norris, G. A.: Methods for estimating uncertainty in factor analytic solutions, Atmos. Meas. Tech., 7, 781-797, doi: 10.5194/amt-7-781-2014, 2014.

Pan, Y., Wang, Y., Sun, Y., Tian, S., and Cheng, M.: Size-resolved aerosol trace elements at a rural mountainous site in Northern China: Importance of regional transport, Sci. Total Environ., 461–462, 761-771, doi: 10.1016/j.scitotenv.2013.04.065, 2013.

Pey, J., Pérez, N., Cortés, J., Alastuey, A., and Querol, X.: Chemical fingerprint and impact of shipping emissions over a western Mediterranean metropolis: Primary and aged contributions, Sci. Total Environ., 463-464, 497-507, doi: 10.1016/j.scitotenv.2013.06.061, 2013.

Pui, D. Y. H., Chen, S.-C., and Zuo, Z.: $PM_{2.5}$ in China: Measurements, sources, visibility and health effects, and mitigation, Particuology, 13, 1-26, doi: 10.1016/j.partic.2013.11.001, 2014.

Shahsavani, A., Naddafi, K., Jaafarzadeh Haghighifard, N., Mesdaghinia, A., Yunesian, M., Nabizadeh, R., Arhami, M., Yarahmadi, M., Sowlat, M. H., Ghani, M., Jonidi Jafari, A., Alimohamadi, M., Motevalian, S. A.,

and Soleimani, Z.: Characterization of ionic composition of TSP and PM_{10} during the Middle Eastern Dust (MED) storms in Ahvaz, Iran, Environ. Monit. Assess., 184, 6683-6692, doi: 10.1007/s10661-011-2451-6, 2012.

Sheehan, P., Cheng, E., English, A., and Sun, F.: China's response to the air pollution shock, Nat. Clim. Change, 4, 306-309, doi: 10.1038/nclimate2197, 2014.

Shi, T., Liu, Y., Zhang, L., Hao, L., and Gao, Z.: Burning in agricultural landscapes: an emerging natural and human issue in China, Landsc. Ecol., 29, 1785-1798, doi: 10.1007/s10980-014-0060-9, 2014a.

Shi, Y., Xia, Y.-f., Lu, B.-h., Liu, N., Zhang, L., Li, S.-j., and Li, W.: Emission inventory and trends of NOx for China, 2000–2020, J. Zheijang Univ.-Sci., 15, 454-464, doi: 10.1631/jzus.A1300379, 2014b.

Szidat, S., Jenk, T. M., Gäggeler, H. W., Synal, H. A., Fisseha, R., Baltensperger, U., Kalberer, M., Samburova, V., Reimann, S., Kasper-Giebl, A., and Hajdas, I.: Radiocarbon (^{14}C)-deduced biogenic and anthropogenic contributions to organic carbon (OC) of urban aerosols from Zürich, Switzerland, Atmos. Environ., 38, 4035-4044, doi: 10.1016/j.atmosenv.2004.03.066, 2004.

Szidat, S.: Sources of Asian Haze, Science, 323, 470-471, doi: 10.1126/science.1169407, 2009.

Tan, J., Duan, J., Zhen, N., He, K., and Hao, J.: Chemical characteristics and source of size-fractionated atmospheric particle in haze episode in Beijing, Atmos. Res., 167, 24-33, doi: 10.1016/j.atmosres.2015.06.015, 2016.

Tao, J., Gao, J., Zhang, L., Zhang, R., Che, H., Zhang, Z., Lin, Z., Jing, J., Cao, J., and Hsu, S. C.: $PM_{2.5}$ pollution in a megacity of southwest China: source apportionment and implication, Atmos. Chem. Phys., 14, 8679-8699, doi: 10.5194/acp-14-8679-2014, 2014.

Tian, S., Pan, Y., Liu, Z., Wen, T., and Wang, Y.: Size-resolved aerosol chemical analysis of extreme haze pollution events during early 2013 in urban Beijing, China, J. Hazard. Mater., 279, 452-460, doi:

10.1016/j.jhazmat.2014.07.023, 2014.

Wacker, L., Fahrni, S. M., Hajdas, I., Molnar, M., Synal, H. A., Szidat, S., and Zhang, Y. L.: A versatile gas interface for routine radiocarbon analysis with a gas ion source, Nucl. Instrum. Methods Phys. Res., Sect. B, 294, 315-319, doi: 10.1016/j.nimb.2012.02.009, 2013.

Wang, X., Bi, X., Sheng, G., and Fu, J.: Hospital indoor PM_{10}/$PM_{2.5}$ and associated trace elements in Guangzhou, China, Sci. Total Environ., 366, 124-135, doi: 10.1016/j.scitotenv.2005.09.004, 2006.

Wang, X., Chen, Y., Tian, C., Huang, G., Fang, Y., Zhang, F., Zong, Z., Li, J., and Zhang, G.: Impact of agricultural waste burning in the Shandong Peninsula on carbonaceous aerosols in the Bohai Rim, China, Sci. Total Environ., 481, 311-316, doi: 10.1016/j.scitotenv.2014.02.064, 2014.

Wang, Y., Zhuang, G. S., Tang, A. H., Yuan, H., Sun, Y. L., Chen, S. A., and Zheng, A. H.: The ion chemistry and the source of $PM_{2.5}$ aerosol in Beijing, Atmos. Environ., 39, 3771-3784, doi: 10.1016/j.atmosenv.2005.03.013, 2005.

Weber, R. J., Sullivan, A. P., Peltier, R. E., Russell, A., Yan, B., Zheng, M., de Gouw, J., Warneke, C., Brock, C., Holloway, J. S., Atlas, E. L., and Edgerton, E.: A study of secondary organic aerosol formation in the anthropogenic-influenced southeastern United States, J. Geophys. Res. Atmos., 112, D13302, doi: 10.1029/2007JD008408, 2007.

Wilson, T. W., Ladino, L. A., Alpert, P. A., Breckels, M. N., Brooks, I. M., Browse, J., Burrows, S. M., Carslaw, K. S., Huffman, J. A., Judd, C., Kilthau, W. P., Mason, R. H., McFiggans, G., Miller, L. A., Najera, J. J., Polishchuk, E., Rae, S., Schiller, C. L., Si, M., Temprado, J. V., Whale, T. F., Wong, J. P. S., Wurl, O., Yakobi-Hancock, J. D., Abbatt, J. P. D., Aller, J. Y., Bertram, A. K., Knopf, D. A., and Murray, B. J.: A marine biogenic source of atmospheric ice-nucleating particles, Nature, 525, 234-238, doi: 10.1038/nature14986, 2015.

Xu, X., Trumbore, S. E., Zheng, S., Southon, J. R., McDuffee, K. E., Luttgen, M., and Liu, J. C.: Modifying a sealed tube zinc reduction method for preparation of AMS graphite targets: Reducing background and attaining high precision, Nucl. Instrum. Methods Phys. Res., Sect. B, 259, 320-329, doi: 10.1016/j.nimb.2007.01.175, 2007.

Yang, F., Tan, J., Zhao, Q., Du, Z., He, K., Ma, Y., Duan, F., and Chen, G.: Characteristics of $PM_{2.5}$ speciation in representative megacities and across China, Atmos. Chem. Phys., 11, 5207-5219, doi: 10.5194/acp-11-5207-2011, 2011.

Zhang, F., Chen, Y., Tian, C., Wang, X., Huang, G., Fang, Y., and Zong, Z.: Identification and quantification of shipping emissions in Bohai Rim, China, Sci. Total Environ., 497–498, 570-577, doi: 10.1016/j.scitotenv.2014.08.016, 2014a.

Zhang, R., Jing, J., Tao, J., Hsu, S. C., Wang, G., Cao, J., Lee, C. S. L., Zhu, L., Chen, Z., Zhao, Y., and Shen, Z.: Chemical characterization and source apportionment of $PM_{2.5}$ in Beijing: seasonal perspective, Atmos. Chem. Phys., 13, 7053-7074, doi: 10.5194/acp-13-7053-2013, 2013.

Zhang, S., Wu, Y., Wu, X., Li, M., Ge, Y., Liang, B., Xu, Y., Zhou, Y., Liu, H., Fu, L., and Hao, J.: Historic and future trends of vehicle emissions in Beijing, 1998–2020: A policy assessment for the most stringent vehicle emission control program in China, Atmos. Environ., 89, 216-229, doi: 10.1016/j.atmosenv.2013.12.002, 2014b.

Zhang, Y.-L., Li, J., Zhang, G., Zotter, P., Huang, R.-J., Tang, J.-H., Wacker, L., Prévôt, A. S. H., and Szidat, S.: Radiocarbon-based source apportionment of carbonaceous aerosols at a regional background site on Hainan Island, South China, Environ. Sci. Technol., 48, 2651-2659, doi: 10.1021/es4050852, 2014c.

Zhang, Y.-L., and Cao, F.: Is it time to tackle $PM_{2.5}$ air pollutions in China from biomass-burning emissions?, Environ. Pollut., 202, 217-219, doi: 10.1016/j.envpol.2015.02.005, 2015.

Zhang, Y. L., Liu, D., Shen, C. D., Ding, P., and Zhang, G.: Development of a preparation system for the radiocarbon analysis of organic carbon in carbonaceous aerosols in China, Nucl. Instrum. Methods Phys. Res., Sect. B, 268, 2831-2834, doi: 10.1016/j.nimb.2010.06.032, 2010.

Zhang, Y. L., Huang, R. J., El Haddad, I., Ho, K. F., Cao, J. J., Han, Y., Zotter, P., Bozzetti, C., Daellenbach, K. R., Canonaco, F., Slowik, J. G., Salazar, G., Schwikowski, M., Schnelle-Kreis, J., Abbaszade, G., Zimmermann, R., Baltensperger, U., Prévôt, A. S. H., and Szidat, S.: Fossil vs. non-fossil sources of fine carbonaceous aerosols in four Chinese cities during the extreme winter haze episode of 2013, Atmos. Chem. Phys., 15, 1299-1312, doi: 10.5194/acp-15-1299-2015, 2015.

Zhao, B., Wang, P., Ma, J. Z., Zhu, S., Pozzer, A., and Li, W.: A high-resolution emission inventory of primary pollutants for the Huabei region, China, Atmos. Chem. Phys., 12, 481-501, doi: 10.5194/acp-12-481-2012, 2012.

Zhao, P. S., Dong, F., He, D., Zhao, X. J., Zhang, X. L., Zhang, W. Z., Yao, Q., and Liu, H. Y.: Characteristics of concentrations and chemical compositions for $PM_{2.5}$ in the region of Beijing, Tianjin, and Hebei, China, Atmos. Chem. Phys., 13, 4631-4644, doi: 10.5194/acp-13-4631-2013, 2013.

Zhou, Y., Cheng, S., Lang, J., Chen, D., Zhao, B., Liu, C., Xu, R., and Li, T.: A comprehensive ammonia emission inventory with high-resolution and its evaluation in the Beijing–Tianjin–Hebei (BTH) region, China, Atmos. Environ., 106, 305-317, doi: 10.1016/j.atmosenv.2015.01.069, 2015.

Zong, Z., Chen, Y., Tian, C., Fang, Y., Wang, X., Huang, G., Zhang, F., Li, J., and Zhang, G.: Radiocarbon-based impact assessment of open biomass burning on regional carbonaceous aerosols in North China, Sci. Total Environ., 518–519, 1-7, doi: 10.1016/j.scitotenv.2015.01.113, 2015.

Table 1. Statistics of $PM_{2.5}$ chemical components on the Qimu Island during the sampling period

Species	Mean ± std. ($\mu g\ m^{-3}$)	Range ($\mu g\ m^{-3}$)	Species	Mean ± std ($ng\ m^{-3}$)	Range ($ng\ m^{-3}$)
$PM_{2.5}$	77.6 ± 59.3	12.7 – 305	Fe	408 ± 285	7.12 – 1588
SO_4^{2-}	14.2 ± 18.0	1.37 – 96.2	Zn	107 ± 142	5.56 – 987
NO_3^-	11.9 ± 16.4	0.27 – 87.1	Pb	88.4 ± 85.7	3.02 – 412
NH_4^+	3.11 ± 2.14	0.61 – 10.1	Mn	29.3 ± 28.0	1.38 – 108
Cl^-	2.06 ± 1.78	0.10 – 8.90	Cu	9.08 ± 11.4	0.03 – 77.7
K^+	0.96 ± 0.84	0.07 – 3.95	Ti	7.72 ± 7.34	0.01 – 30.7
Na^+	0.43 ± 0.25	0.05 – 1.58	As	6.61 ± 7.86	0.67 – 43.4
Ca^{2+}	0.38 ± 0.22	0.07 – 1.32	Ni	4.28 ± 2.30	1.68 – 13.8
Mg^{2+}	0.03 ± 0.03	0.01 – 0.17	V	3.90 ± 2.47	0.45 – 12.5
OC	6.85 ± 4.81	0.81 – 21.3	Cd	1.82 ± 4.06	0.04 – 25.9
EC	4.90 ± 4.11	0.80 – 19.6	Co	0.24 ± 0.18	0.01 – 0.73

Table 2. Statistics of $PM_{2.5}$ chemical species in different clusters and significant level by mean test

Species (unit)	Mean ± standard deviation (range) Cluster1(n=42)	Cluster2(n=25)	Cluster3(n=9)	Significant level 1&2	1&3	2&3
$PM_{2.5}$ ($\mu g\ m^{-3}$)	93.0 ± 66.1 (24.5–305)	41.6 ±26.7 (12.7–143)	106 ±42.3 (50.3–193)	0.00	0.59	0.00
EC ($\mu g\ m^{-3}$)	6.53 ± 4.66 (1.39–19.6)	2.50 ±1.84 (0.80–8.85)	3.94 ±1.49 (2.53–7.66)	0.00	0.11	0.05
OC ($\mu g\ m^{-3}$)	8.58 ± 5.23 (1.45–21.3)	3.51 ±2.35 (0.81–11.4)	8.04 ±2.32 (5.25–13.5)	0.00	0.76	0.00
Cl^- ($\mu g\ m^{-3}$)	2.37 ± 2.11 (0.10–8.90)	1.22 ±0.65 (0.20–2.85)	2.94 ±1.35 (1.42–5.53)	0.01	0.45	0.00
NO_3^- ($\mu g\ m^{-3}$)	17.6 ± 19.6 (1.75–87.0)	2.75 ±4.25 (0.27–20.1)	10.6 ±6.09 (4.41–20.3)	0.00	0.30	0.00
SO_4^{2-} ($\mu g\ m^{-3}$)	19.4 ± 21.8 (2.09–96.2)	4.55 ±4.06 (1.37–19.5)	16.4 ±8.74 (5.34–35.6)	0.00	0.69	0.00
Na^+ ($\mu g\ m^{-3}$)	0.38 ± 0.24 (0.05–1.58)	0.55 ±0.26 (0.18–1.08)	0.31 ±0.06 (0.22–0.40)	0.01	0.41	0.01
NH_4^+ ($\mu g\ m^{-3}$)	3.97 ± 2.29 (1.28–10.1)	1.53 ±0.98 (0.61–4.70)	3.52 ±0.96 (1.93–4.90)	0.00	0.57	0.00
K^+ ($\mu g\ m^{-3}$)	1.11 ± 0.74 (0.28–3.10)	0.35 ±0.36 (0.07–1.69)	2.01 ±0.93 (0.78–3.95)	0.00	0.00	0.00
Mg^{2+} ($\mu g\ m^{-3}$)	0.03 ± 0.03 (0.01–0.17)	0.03 ±0.02 (0.01–0.11)	0.02 ±0.01 (0.01–0.04)	0.66	0.41	0.13
Ca^{2+} ($\mu g\ m^{-3}$)	0.37 ± 0.22 (0.11–1.32)	0.37 ±0.18 (0.07–0.74)	0.44 ±0.29 (0.09–0.97)	1.00	0.46	0.46
Ti ($ng\ m^{-3}$)	6.96 ± 5.98 (0.35–25.9)	10.9 ±9.10 (0.01–30.7)	2.51 ±0.85 (1.16–3.58)	0.04	0.03	0.01
V ($ng\ m^{-3}$)	4.68 ± 2.29 (0.76–11.3)	2.83 ±2.55 (0.45–12.4)	3.24 ±1.50 (2.05–7.12)	0.00	0.08	0.66
Mn ($ng\ m^{-3}$)	33.8 ± 31.3 (1.97–108)	17.6 ±19.3 (1.38–95.4)	40.9 ±20.3 (9.14–69.8)	0.02	0.53	0.01
Fe ($ng\ m^{-3}$)	404 ± 308 (7.12–1588)	375 ±263 (9.13–826)	521 ±188 (244–960)	0.70	0.29	0.15
Co ($ng\ m^{-3}$)	0.26 ± 0.20 (0.01–0.73)	0.17 ±0.14 (0.01–0.48)	0.36 ±0.13 (0.10–0.59)	0.08	0.14	0.00
Ni ($ng\ m^{-3}$)	4.85 ± 2.56 (1.68–13.8)	3.51 ±1.85 (1.68–6.79)	3.80 ±1.02 (2.45–5.84)	0.03	0.24	0.67
Cu ($ng\ m^{-3}$)	11.6 ± 13.6 (0.72–77.7)	3.06 ±2.93 (0.03–8.99)	13.9 ±7.05 (3.90–26.4)	0.00	0.64	0.00
Zn ($ng\ m^{-3}$)	146 ± 176 (9.92–987)	46.4 ±50.1 (5.56–208)	90.4 ±47.4 (24.2–201)	0.01	0.36	0.03
As ($ng\ m^{-3}$)	9.03 ± 9.52 (1.11–43.4)	3.00 ±2.82 (0.67–14.0)	5.35 ±3.35 (2.25–13.6)	0.00	0.27	0.06
Cd ($ng\ m^{-3}$)	2.70 ± 5.26 (0.11–25.9)	0.45 ±0.41 (0.04–1.29)	1.54 ±0.65 (0.49–2.66)	0.04	0.52	0.00
Pb ($ng\ m^{-3}$)	110 ± 95.3 (5.30–412)	36.9 ±44.8 (3.02–176)	128 ±53.2 (45.4–215)	0.00	0.59	0.00

Table 3. Concentration and contemporary carbon fraction of carbonaceous species in M1 and M2

	M1	M2		M1	M2
$PM_{2.5}$ (μg m^{-3})	159.2 ±0.5	91.8 ±0.5			
OC (μg m^{-3})	12.7 ±0.7	9.0 ±0.5	f_c (OC)	0.59 ±0.04	0.46 ±0.04
WSOC (μg m^{-3})	6.4 ±0.4	3.7 ±0.2	f_c (WSOC)	0.59 ±0.03	0.49 ±0.03
WIOC (μg m^{-3})	6.3 ±0.6	5.3 ±0.4	f_c (WIOC)	0.60 ±0.03	0.43 ±0.03
EC (μg m^{-3})	8.6 ±0.5	5.8 ±0.3	f_c (EC)	0.52 ±0.02	0.38 ±0.01

5

Table 4. Averages of fractional contributions (%) from eight sources identified by PMF model

	Vehicle emission	Traffic dust	Ship emission	Industrial process	Biomass burning	Mineral dust	Coal combustion	Sea salt
All	15.83	4.24	8.95	2.64	19.31	12.81	29.64	6.58
Cluster1	23.64	4.89	8.79	3.64	19.61	6.32	29.16	3.96
Cluster2	3.57	3.60	9.34	1.19	4.88	26.81	37.66	12.95
Cluster3	12.46	3.08	8.67	1.96	52.67	6.46	12.38	2.32

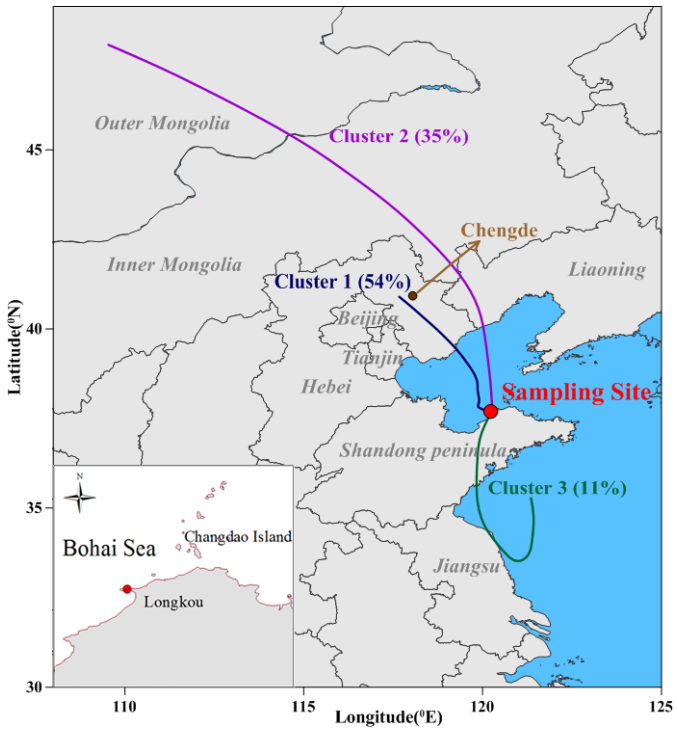

Figure 1. The sampling site and 48-h back trajectory clusters during the sampling period

Figure 2. 48-h back trajectories with 12 h intervals of the combined samples (M1 and M2) selected for ^{14}C analysis. M1 were collected continually from 06:00 to 18:00, 16th January and from 18:00 to 06:00 the next day, when the air masses were derived from the south and passed through the Shandong Peninsula; M2 were collected continually from 17th January 18:00 to 6:00 and from 06:00 to 18:00 in the next day, when the air masses come from the north and reflected the BTH pattern. (The digit in the figure is date and time with the format of YYYYMMDDHH, the time is local time).

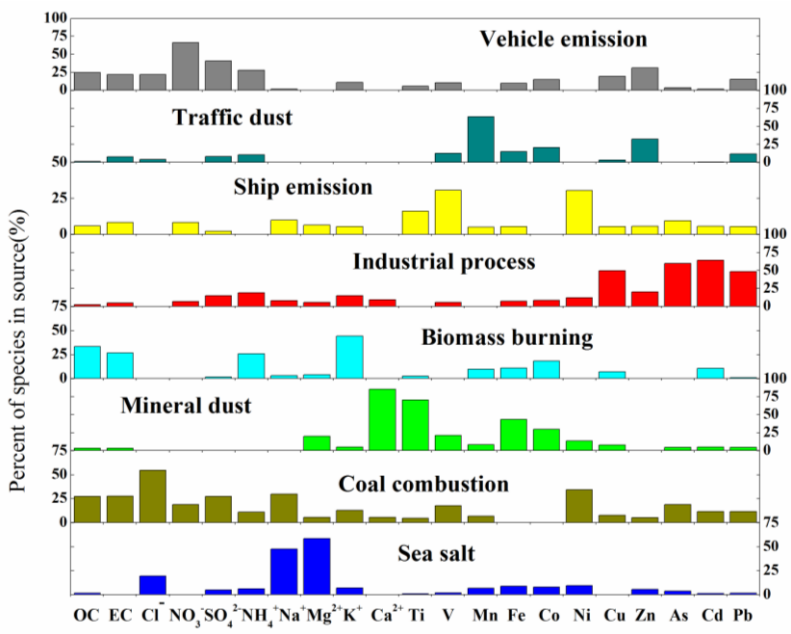

Figure 3. The contribution profiles of eight sources identified by PMF model

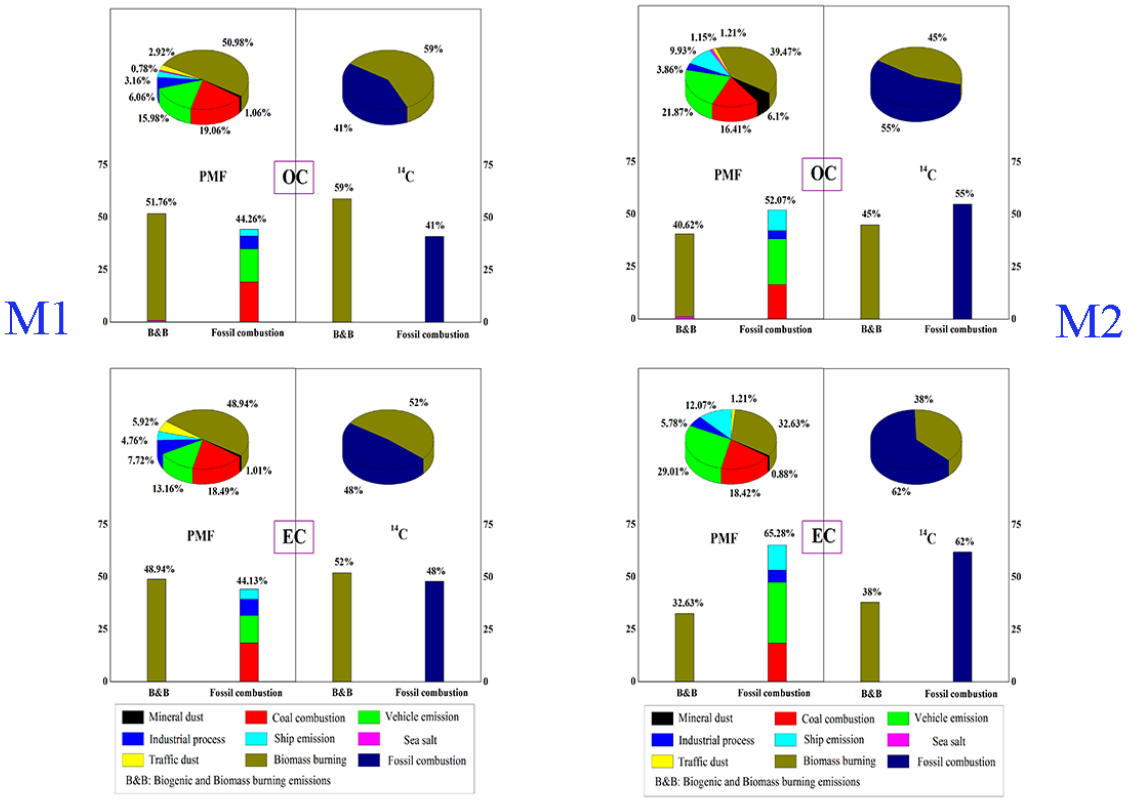

Figure 4. Comparison of source apportionment of OC and EC in the two specified samples (M1 and M2) from PMF and ^{14}C measurement. B&B refers to the source of biogenic and biomass burning. Note: the B&B and Fossil emissions from the PMF result do not add to a hundred in the bars because hybrid sources from B&B and fossil fuel combustion were not be considered in the comparison (mineral dust and vehicle dust).